



Tri-Stereo Model Orientation of High-Resolution Satellite Imagery Combining Ground Control Points and Lines

JINSHAN CAO, XIUXIAO YUAN & YI FANG, Wuhan, China

Keywords: orientation, tri-stereo model, high-resolution satellite imagery, ground control lines, rational function model

Summary: An effective tri-stereo model orientation approach for high-resolution satellite imagery (HRSI) combining ground control points (GCPs) and ground control lines (GCLs) is presented. For the presented approach, both the point-based and the line-based orientation models employ the rational function model rather than the physical sensor model as the geometric imaging model of HRSI. As the parameters of a rational model are frequently distributed with HRSI data, our model is more convenient and practicable for users. The experimental results of two ZiYuan-3 (ZY-3) datasets have shown that in images where it is difficult to identify sufficient and well-distributed GCPs, GCLs can be employed to substitute for the absent GCPs. More specifically, an accuracy better than the ground sample distance (GSD) can be achieved after the tri-stereo model orientation combining three GCPs and one GCL, two GCPs and two GCLs, or one GCP and five GCLs. Additionally, if only GCLs are taken as the control information in the HRSI orientation, a satisfactory accuracy of better than 1 GSD can also be achieved using eight GCLs of appropriate orientations near the image boundaries.

Zusammenfassung: *Tri-Stereo Modellorientierung von hochaufgelösten Satellitenszenen mit einem kombinierten Passpunkt- und Passlinienverfahren.* In diesem Beitrag wird ein effektiver Ansatz zur Modellorientierung von Tripeln von überlappenden hoch aufgelösten Satellitenbildern vorgestellt, welcher Passpunkte (PP) mit Passlinien (PL) kombiniert. Dabei beruhen weder die punkt- noch die linienbasierten Orientierung auf einem physikalischen Sensormodell, sondern auf einem Modell auf der Basis von rationalen Funktionen. Da die Parameter eines Modells auf Basis von rationalen Funktionen häufig mit den Satellitendaten mitgeliefert werden, ist dieses Modell für Anwender einfacher zu nutzen. Die Ergebnisse von Experimenten mit zwei Bildtripeln, die vom Satelliten ZiYuan-3 (ZY-3) aus aufgenommen wurden, haben gezeigt, dass in Bildern, in denen es schwierig ist, eine ausreichende Anzahl von PP mit einer guten räumlichen Verteilung zu identifizieren, PL ein guter Ersatz für PP sein können. Insbesondere wird gezeigt, dass eine Genauigkeit, die besser als die Bodenauflösung (Ground Sampling Distance, GSD) der Bilder ist, erreicht werden kann, wenn drei PP mit einer PL, zwei PP mit zwei PL oder ein PP mit fünf PL kombiniert werden. Selbst wenn keine PP zur Verfügung steht, kann die Orientierung eines Bildtripels mit einer Genauigkeit besser als 1 GSD erfolgen, wenn mindestens acht PL in der Nähe der Bildränder mit geeigneter Verteilung vorliegen.

1 Introduction

Precise orientation is a prerequisite for many applications of high-resolution satellite imagery (HRSI). The orientation accuracy determines the geometric quality of the products derived from HRSI, such as digital elevation models (DEM) and digital orthophoto maps

(DOM). At present, HRSI orientation usually takes ground control points (GCPs) as the control information to relate image space and object space (GRODECKI & DIAL 2003, FRASER & HANLEY 2005, FRASER et al. 2006). The GCPs are mainly surveyed in the field or extracted from the reference DOM and DEM. However, due to the lack of clear point features in the

field or the large time interval between the acquisition of the HRSI and the reference DOM and DEM, it may be very difficult to identify sufficient, evenly distributed and highly accurate GCPs in the areas covered by an image. In these cases, the image orientation using both GCPs and ground control lines (GCLs) can offer an alternative solution for precise orientation.

The use of linear features is not a recent advancement in photogrammetry. MASRY (1981) already presented the original idea in 1981. Compared with point features, linear features are preferred in photogrammetry mainly due to the following reasons (HABIB et al. 2004, SCHENK 2004, KARJALAINEN et al. 2006): (1) Control information in object space is more readily available in the form of linear features for the purpose of the image orientation. (2) Linear features can be easily identified in the image. (3) Information from linear features can be used even without a complete match between image and object linear features. (4) Linear features form a good basis for the automation of photogrammetric processes.

With respect to the HRSI orientation using only GCPs, a lot of research has been done, such as GRODECKI & DIAL (2003), FRASER & HANLEY (2005), FRASER et al. (2006) and ZHANG et al. (2009). This is also true for applications of linear features in photogrammetry. In aerial photogrammetry, linear features were used successfully in the relative orientation, exterior orientation and aerial triangulation (ZHANG et al. 2011, KARJALAINEN et al. 2006, HABIB et al. 2003, SCHENK, 2004). In space photogrammetry, SHI & SHAKER (2006) established a line-based transformation model, whose structure is similar to some point-based transformation models, for image-to-image registration. HABIB & ALRUZOUQ (2004) used linear features as the registration primitives to perform automatic image registration of multi-source satellite images. The approach was shown to be feasible and robust even without a complete correspondence between the registration primitives in the reference and input images. ZHANG et al. (2004) performed an automatic exterior orientation of SPOT-3 images using GCLs and achieved an orientation accuracy of about 1.5 pixels. TOMMASELLI & MEDEIROS (2010) presented an experimental

assessment of both the line-coplanarity model and the adapted equivalent planes model for the indirect orientation of CBERS-2 images using GCLs. The experimental results showed that an accuracy of about twice the ground sample distance (GSD) at independent check points (ICPs) can be achieved. TOMMASELLI & MARCATO JUNIOR (2012) and MARCATO JUNIOR & TOMMASELLI (2013) combined GCPs, GCLs, and orbital data to perform the block adjustment of CBERS-2B images. It was observed that the combination of GCPs and GCLs could provide better results than the conventional bundle block adjustment using only GCPs.

For the orientation of remote sensing imagery using GCLs, as in aerial or space photogrammetry, the most important thing is to establish a mathematical model relating image space and object space. The present line-based models for HRSI orientation can be mainly divided into two categories: the collinearity model and the coplanarity model, the latter being preferred in space photogrammetry (TOMMASELLI & MEDEIROS 2010). In order to establish the coplanarity model, the satellite's position and attitude observations and sensor parameters are indispensable. However, many HRSI satellites, such as IKONOS, GeoEye-1, and ZiYuan-3 (ZY-3), only provide the users with rational polynomial coefficients (RPCs; FRASER et al. 2006) rather than the satellite's position and attitude observations and sensor parameters. In other words, users can only establish the rational functional model (RFM) according to the RPCs, and it is very difficult and even impossible for them to perform HRSI orientation using GCLs based on the coplanarity model. Therefore, a line-based orientation model for the RFM is established and a tri-stereo model orientation approach for HRSI combining GCPs and GCLs is presented in this paper. For the presented approach, only the RPCs rather than the satellite's position and attitude observations and sensor parameters are necessary, so that it is more convenient and practicable for HRSI users. The paper is organised in four sections. In the next section, both the point-based and line-based orientation models are established, and the solutions for the unknowns are introduced briefly. In the following section, the experiments with two ZY-3 datasets are performed to val-

idate the feasibility and effectiveness of the tri-stereo model orientation both using GCLs only and combining GCPs and GCLs. Finally, conclusions are provided.

2 Orientation Models and Solutions

When performing the RFM-based tri-stereo model orientation combining GCPs and GCLs, both GCPs and GCLs are employed as the control information and tie points are used to supply internal geometric constraints between the adjacent satellite images. Hence, the mathematical models of image orientation can be classified into two categories: the point-based orientation model and the line-based orientation model.

2.1 Point-based Orientation Model

For HRSI orientation using point features, the RFM with additional affine transformation parameters (ATPs) is usually employed as the mathematical model. In the RFM, the image point coordinates (r, c) are expressed as the ratios of polynomials of the reduced object point coordinates (X_n, Y_n, Z_n):

$$\begin{cases} r_n = \frac{P_1(X_n, Y_n, Z_n)}{P_2(X_n, Y_n, Z_n)} \\ c_n = \frac{P_3(X_n, Y_n, Z_n)}{P_4(X_n, Y_n, Z_n)} \end{cases} \quad (1)$$

where (r_n, c_n) are the normalized values of the image point coordinates (r, c), whereas the normalised object coordinates are determined from the original object point coordinates (X, Y, Z). The normalization of the coordinates is carried out in the way described in TAO & HU (2001). $P_i(X_n, Y_n, Z_n)(i = 1, 2, 3, 4)$ are the third-order polynomials with X_n, Y_n and Z_n as the independent variables.

Research has shown that using the RFM to fit the physical sensor model (PSM) with the terrain-independent scenario can achieve a very high accuracy and the fitting errors can be ignored (TAO & HU 2001, YUAN & LIN 2008, NAGASUBRAMANIAN et al. 2007). Using

the RFM instead of the PSM to perform image orientation, feature extraction, orthorectification and three-dimensional reconstruction is entirely feasible (FRASER et al. 2002, TAO et al. 2004). However, in order to achieve the best orientation results, the absolute orientation has to be improved. Therefore, the point-based orientation model is actually the bias corrected RPC-solution with two-dimensional affine transformation as follows:

$$\begin{cases} r + e_0 + e_1 r + e_2 c = \frac{P_1(X_n, Y_n, Z_n)}{P_2(X_n, Y_n, Z_n)} r_s + r_o \\ c + f_0 + f_1 r + f_2 c = \frac{P_3(X_n, Y_n, Z_n)}{P_4(X_n, Y_n, Z_n)} c_s + c_o \end{cases} \quad (2)$$

where (r_o, c_o) and (r_s, c_s) are, respectively, the offset values and scaling values of the image point coordinates; ($e_0, e_1, e_2, f_0, f_1, f_2$) are the ATPs and ($e_0 + e_1 r + e_2 c, f_0 + f_1 r + f_2 c$) can be considered as the error correction values of the image point coordinates.

2.2 Line-based Orientation Model

As shown in Fig. 1, a straight line L in object space is determined by two points P_1 and P_2 , whose object coordinates are known. The straight line l_T in image space corresponds to L , and the point t is an arbitrary point on the line l_T . A straight line l_p in image space is determined by the image points p_1 and p_2 , which can be obtained by projecting the points P_1 and P_2 into the image according to (1). In this paper, the line l_T is called the ‘‘observed line’’ and the line l_p is called the ‘‘projected line’’.

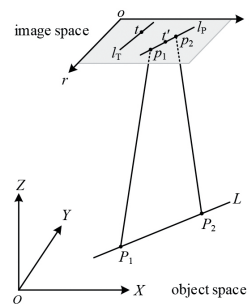


Fig. 1: Relation between linear features in object space and in HRSI.

If the RPCs do not contain systematic errors, the observed line l_T and the projected line l_p are bound to coincide, that is, the point t is bound to lie on the line l_p . In reality, however, the point t will deviate from the line l_p , resulting from the influence of the systematic errors in the RPCs. Therefore, the ATPs according to (2) should be determined so that after the correction of its image coordinates the geometric constraint that the point t lies on the line l_p is satisfied.

Suppose that the point t' in Fig. 1 is obtained by correcting the systematic errors of the point t , and then the point t' should lie on the line l_p . Additionally, the image coordinates of the points t and t' satisfy the two-dimensional affine transformation as follows:

$$\begin{cases} r_{t'} = r_t + e_0 + e_1 r_t + e_2 c_t \\ c_{t'} = c_t + f_0 + f_1 r_t + f_2 c_t \end{cases} \quad (3)$$

where (r_t, c_t) and $(r_{t'}, c_{t'})$ are, respectively, the image coordinates of the points t and t' and the coefficients e_j, f_j are the ATPs also defined in (2).

A straight line in image space has several mathematical expressions, such as slope-intercept form, point-slope form and two-point form. In this paper, the slope-intercept form is

$$r_t = -e_0 - r_t e_1 - c_t e_2 + k f_0 + k r_t f_1 + k c_t f_2 + k c_t + b \quad (8)$$

$$c_t = k e_0 + k r_t e_1 + k c_t e_2 - f_0 - r_t f_1 - c_t f_2 + k r_t + b \quad (9)$$

The point t in image space is an arbitrary point on the observed line l_T rather than the corresponding point of one of the object points P_1 or P_2 . Therefore, when establishing the line-based orientation model, the point on the image line does not have to correspond with a specific point on the object line, but only the correspondence between the image line and the object line is necessary. Consequently, linear features are preferable to point features in areas where GCPs are difficult to be identified.

2.3 Simultaneous Adjustment

From (8) and (9), it can be seen that no additional unknowns are introduced when establishing the line-based orientation model using GCLs. Therefore, when performing the

employed to express the line l_p , so as to establish the line-based orientation model conveniently. Meanwhile, taking into account the influence of the line slope on the image orientation, the lines in image space are divided into two types according to the angle θ between the line and the c -axis of the image coordinate system $o-rc$, as shown in Fig. 2. If the angle θ satisfies the condition $-45^\circ \leq \theta \leq 45^\circ$, (4) is employed to express line l_p ; otherwise, (5) is used:

$$r = kc + b \quad (4)$$

$$c = kr + b \quad (5)$$

In (4) and (5), k and b are the slope and the intercept, respectively, of the line l_p , which can be obtained from the image coordinates of the points p_1 and p_2 .

According to the geometric constraint that the point t' lies on the line l_p , the image coordinates of the point t' should satisfy (4) or (5), so (6) and (7) can be obtained:

$$r_{t'} = k c_{t'} + b \quad (6)$$

$$c_{t'} = k r_{t'} + b \quad (7)$$

Substituting (3) into (6) and (7), respectively, the line-based orientation model can be established as shown in (8) and (9):

tri-stereo model orientation combining GCPs and GCLs, the unknowns are still the ATPs of each image and the object coordinates of each tie point. In theory, one observation equation, either (8) or (9), can be established for each image point on an observed line l_T . In this paper, only two image points t_1 and t_2 per line l_T are used in the tri-stereo model orientation, since any observed line can be determined by two image points. The general procedure of solving the unknowns is as follows:

(1) For each GCL in each image, the image points p_1 and p_2 are, respectively, obtained by projecting the points P_1 and P_2 observed on the object line L into the image according to (1) and then the slope k and the intercept b of the projected line l_p are computed using the image coordinates of the resultant points p_1 and p_2 . After that, according

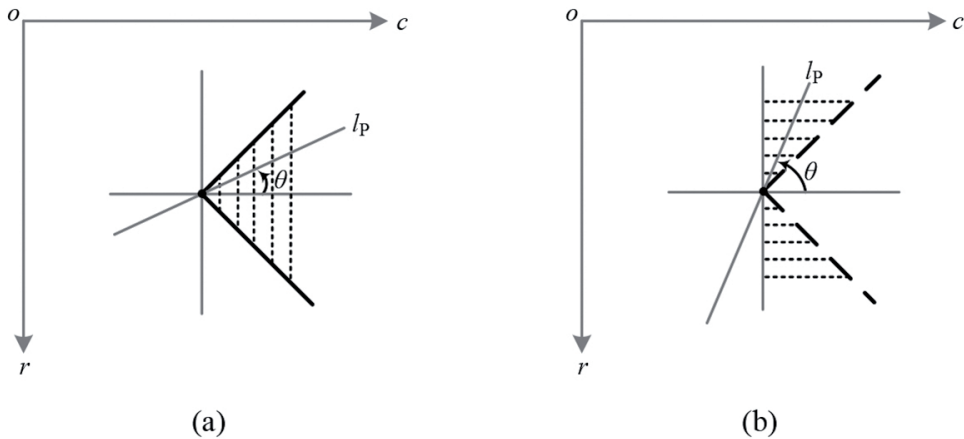


Fig. 2: Two types of straight lines in image space: (a) $-45^\circ \leq \theta \leq 45^\circ$, (b) $45^\circ < \theta < 90^\circ$ and $-90^\circ \leq \theta < -45^\circ$.

to (8) or (9), two error equations are established using the image coordinates of the observed points t_1 and t_2 on the observed line l_p . That is, each of the two points contributes one error equation.

- (2) For each GCP in each image, according to (2), two error equations are established using the observed image and object coordinates of the GCP.
- (3) For each tie point in each image, according to (2), two error equations are established using the observed image coordinates of the tie point.
- (4) Combining the error equations relating to GCLs, GCPs and tie points, the ATPs and the object coordinates of tie points are solved simultaneously by least-squares adjustment.

3 Experimental Results and Analysis

3.1 Experimental Datasets

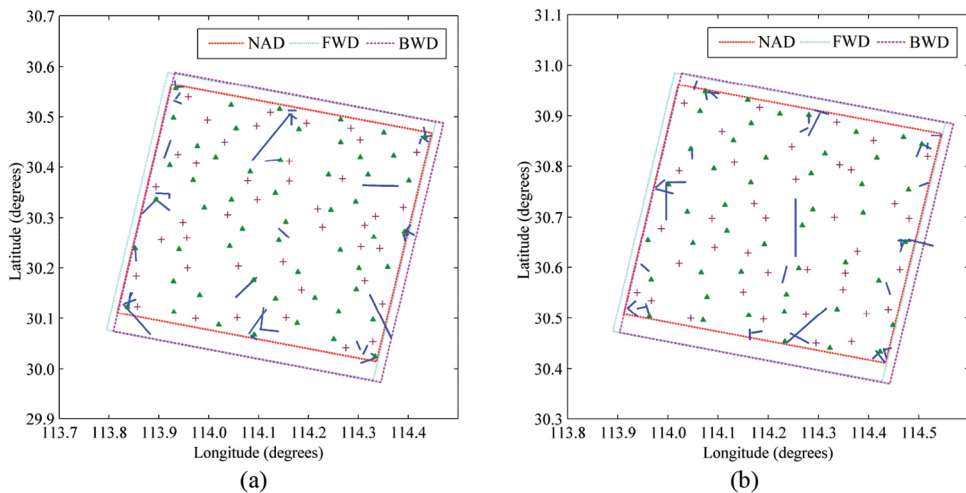
In this study, two sets of ZY-3 three-line camera (TLC) images were tested. The general characteristics of the datasets are depicted in Tab. 1. Both datasets have three images in the forward (FWD), nadir (NAD) and backward (BWD) views, respectively. The GSD of the FWD, NAD and BWD images is about 3.5 m,

2.1 m and 3.5 m, respectively. The swath width of the FWD, NAD and BWD cameras is about 51 km. The FWD and BWD cameras are tilted by $+22^\circ$ and -22° from the NAD camera, respectively, and form a base-to-height ratio of 0.87 with Earth curvature considered. The object coordinates of the GCLs and GCPs in both datasets were measured manually from the reference DOM and DEM. The GSD of the DOM is 0.2 m and the planimetric accuracy is about 1.0 m. The point spacing of the DEM is 1.0 m and the height accuracy is about 2.0 m. The image coordinates of the GCLs and GCPs in every ZY-3 image were also measured manually and the measurement accuracy is about 0.4 pixel. The tie points were extracted and matched automatically in the FWD, NAD and BWD images using the matching algorithm presented in YUAN & LIU (2009). In the following experiments, the FWD, NAD and BWD images in each dataset formed a tri-stereo model, and the tri-stereo model orientation was performed according to the procedure in section 2.3. In the experiments described in sections 3.2 to 3.4, only the GCLs and tie points were used; in section 3.2, results for GCLs and GCPs are compared. In the experiments reported in section 3.5, the GCPs, GCLs and tie points were used.

As shown in Fig. 3, the GCPs, GCLs and tie points are distributed evenly in the areas depicted in the images. The GCLs are mainly road edges and river edges in this paper. When

Tab. 1: General characteristics of the datasets.

Characteristics	Dataset 1	Dataset 2
Geographic area of images	Wuhan, China	Wuhan, China
Number of images	3	3
Acquisition date	20th June 2012	22nd April 2012
Terrain relief	18 to 252 m	16 to 107 m
Number of GCLs	39	39
Number of GCPs	54	47
Number of tie points	41	38

**Fig. 3:** Distributions of the GCPs and GCLs in the: (a) dataset 1, (b) dataset 2. Note that \blacktriangle denotes GCPs, — denotes GCLs, + denotes tie points. For better readability, the lengths of the GCLs were scaled by a factor five.

measuring the GCLs, the object coordinates of the points P_1 and P_2 on a straight line L were determined based on the reference DOM and DEM, and then the image coordinates of the points t_1 and t_2 on the corresponding image line l_T were measured. Note that the two points on the image line need not (and in general do not) correspond with the ones on the line in the reference DOM and DEM.

3.2 Effects of the Number and Distribution of GCLs on the Tri-Stereo Model Orientation Using GCLs

For the tri-stereo model orientation of ZY-3 images, each GCP delivers two observations

and each point on a GCL delivers one observation. Therefore, no less than three GCPs or three GCLs are theoretically required to determine the ATPs. However, when using GCLs, one has to take care that the directions of the lines allow for a solution of the resultant normal equation system; the lengths of the line segments also have an impact on the determinability of the parameters. Furthermore, more observations may be required for obtaining an accurate and numerically stable solution. In this section, in order to firstly analyse the effects of the number and distribution of GCLs on the tri-stereo model orientation, one GCP layout scenario and five different GCL layout scenarios were designed. The layouts are as follows:

- (1) *Layout P4*. Four GCPs in the image corners, as shown in Fig. 4a;
- (2) *Layout L4*. Four GCLs in the image corners, as shown in Fig. 4b;
- (3) *Layout L6*. Six GCLs along the along-track image boundary, as shown in Fig. 4c;
- (4) *Layout L8*. Eight GCLs near the image boundary, as shown in Fig. 4d; and
- (5) *Layout L15*. Eight GCLs near the image boundary and seven GCLs distributed evenly in the image, as shown in Fig. 4e.

the above layout scenarios, and the remaining GCPs were considered as the ICPs. Note that the angles θ of the selected GCLs are distributed evenly in the four angle ranges $[-90^\circ, -45^\circ]$, $[-45^\circ, 0^\circ]$, $[0^\circ, 45^\circ]$ and $(45^\circ, 90^\circ)$, as listed in Tabs. 2 and 3, and the effects of the directions and the lengths of GCLs on the tri-stereo model orientation will be analysed in the following sections. After the tri-stereo model orientation according to the procedure in section 2.3, the root-mean-square errors (RMSE) of the object coordinates at the ICPs were calculated. They are listed in Tabs. 2 and 3.

For each dataset in Fig. 3, the satisfactory GCPs and GCLs were selected according to

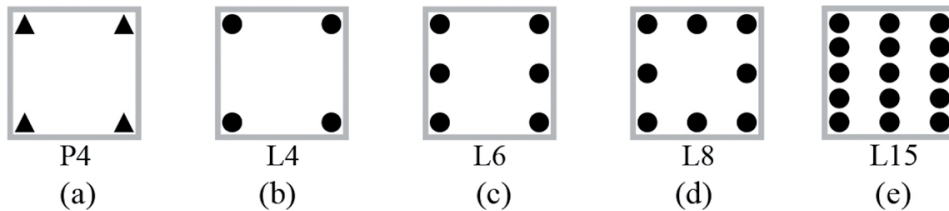


Fig. 4: GCP and GCL layout scenarios: (a) four GCPs, (b) four GCLs, (c) six GCLs, (d) eight GCLs, (e) fifteen GCLs. Note that \blacktriangle denotes GCPs and \bullet denotes GCLs.

Tab. 2: Tri-stereo model orientation results using the GCPs and GCLs in the dataset 1.

Layout	Angles of GCLs in the NAD image ($^\circ$)	Number of ICPs	RMSE (m)			
			North	East	Planimetry	Height
P4	/	50	1.916	2.035	2.795	2.116
L4	-86, -35, 23, 73	54	107.184	60.760	123.208	84.097
L6	-86, -35, 18, 23, 73, 79	54	3.642	3.258	4.887	5.450
L8	-86, -66, -35, -5, 18, 23, 73, 79	54	2.089	2.009	2.899	2.202
L15	-86, -84, -66, -59, -35, -20, -11, -5, 18, 23, 34, 55, 73, 74, 79	54	2.215	1.779	2.841	2.099

Tab. 3: Tri-stereo model orientation results using the GCPs and GCLs in the dataset 2.

Layout	Angles of GCLs in the NAD image ($^\circ$)	Number of ICPs	RMSE (m)			
			North	East	Planimetry	Height
P4	/	43	2.205	1.790	2.840	2.065
L4	-57, -27, 35, 81	47	75.257	56.173	93.909	77.615
L6	-86, -57, -27, 5, 35, 81	47	6.300	2.153	6.658	7.129
L8	-86, -57, -42, -27, 5, 19, 35, 81	47	1.904	1.978	2.745	2.083
L15	-89, -86, -57, -57, -42, -35, -27, 5, 19, 33, 35, 61, 77, 78, 81	47	1.582	2.210	2.718	2.090

From the results in Tabs. 2 and 3, the following four conclusions can be drawn. First, the orientation accuracy achieved using four GCLs in the layout L4 is much worse than the one achieved using four GCPs, even if the angles of the GCLs are distributed evenly in the four angle ranges. In our experiments, the control information provided by four GCLs is insufficient for an accurate tri-stereo model orientation, but this may also be affected by the specific configuration of GCLs with the given directions in the images and with given lengths. The normal equation matrix of the least-squares adjustment is ill-conditioned, and the solved ATPs and the object coordinates of the tie points deviate from their true values. Take the dataset 1 for an example. The standard deviations (SDs) of the solved ATPs of the NAD image even reach values as large as about 80 pixels, as listed in Tab. 4. As a result, the solved ATPs cannot effectively compensate the systematic errors in the RPCs at all. The residual errors of the ICPs are still very large, as shown in Fig. 5a, which is also consistent with the SDs of the tie points in Fig. 6a. Note that the SDs of both, the solved ATPs and the tie points, were derived from the SD of the unit weight and the co-factor matrix after least-squares adjustment.

Second, when using six GCLs in the layout L6 to perform the tri-stereo model orientation, the solved ATPs deviate from the values achieved when using points, as listed in Tab. 4. The orientation accuracies of both datasets are worse than 1 GSD (3.5 m in this paper). The reason is again to be found in the specific arrangement of GCLs in these examples. It is

demonstrated that it is very difficult to achieve the best orientation accuracy using the layout L6, even if the directions of the selected GCLs are distributed evenly.

When eight GCLs are employed as control information (in the layout L8), the deviation of the solved ATPs from the point-based solution can be further reduced and a satisfactory orientation accuracy can be achieved. Again, take the dataset 1 for an example. The SDs of the parameters e_0 and f_0 of the NAD image are better than 0.4 pixel, and the SDs of the other ATPs are better than $1.8E-5$. Accordingly, the residual errors of the ICPs are further reduced, as shown in Fig. 5b, which is also consistent with the SDs of the tie points in Fig. 6b. The orientation accuracy is improved to 2.9 m in planimetry and 2.2 m in height, which is almost the same as the one achieved with the layout P4. It is demonstrated that in order to achieve a good orientation result, at least eight GCLs near the boundary of the areas are necessary, but this result heavily depends on the distribution of the GCL directions.

Finally, the orientation accuracy cannot be improved significantly any more with the number of GCLs increased from eight in the layout L8 to fifteen in the layout L15. For both datasets, the difference between the accuracies achieved with the layouts L8 and L15 is smaller than 0.1 m in planimetry and 0.2 m in height. It means that using more GCLs one can hardly expect large improvements of the orientation accuracy, even if the GCLs are distributed evenly in the areas covered by the images.

Tab. 4: The solved ATPs of the NAD image in the dataset 1.

Layout	e_0 (pixels) (SD)	e_1 (SD)	e_2 (SD)	f_0 (pixels) (SD)	f_1 (SD)	f_2 (SD)
P4	9.519E+0 (2.463E-1)	-9.224E-5 (1.177E-5)	7.626E-6 (1.125E-5)	-8.825E+0 (2.389E-1)	4.280E-5 (1.144E-5)	-1.258E-5 (1.094E-5)
L4	1.505E+1 (7.968E+1)	2.762E-3 (3.335E-3)	-4.642E-3 (1.488E-3)	-5.199E+0 (2.470E+1)	-4.426E-3 (1.779E-3)	4.306E-4 (1.166E-3)
L6	1.444E+1 (8.538E-1)	-2.101E-4 (2.701E-5)	-1.533E-4 (2.665E-5)	-5.751E+0 (3.755E-1)	-2.104E-4 (3.042E-5)	-8.235E-5 (1.675E-5)
L8	9.349E+0 (3.899E-1)	-3.862E-5 (1.314E-5)	-1.210E-5 (1.645E-5)	-7.988E+0 (1.919E-1)	-4.427E-5 (1.787E-5)	1.061E-5 (1.148E-5)
L15	8.627E+0 (2.224E-1)	-2.205E-5 (9.347E-6)	9.420E-6 (9.620E-6)	-7.810E+0 (1.314E-1)	-1.886E-5 (8.561E-6)	-3.965E-6 (7.651E-6)

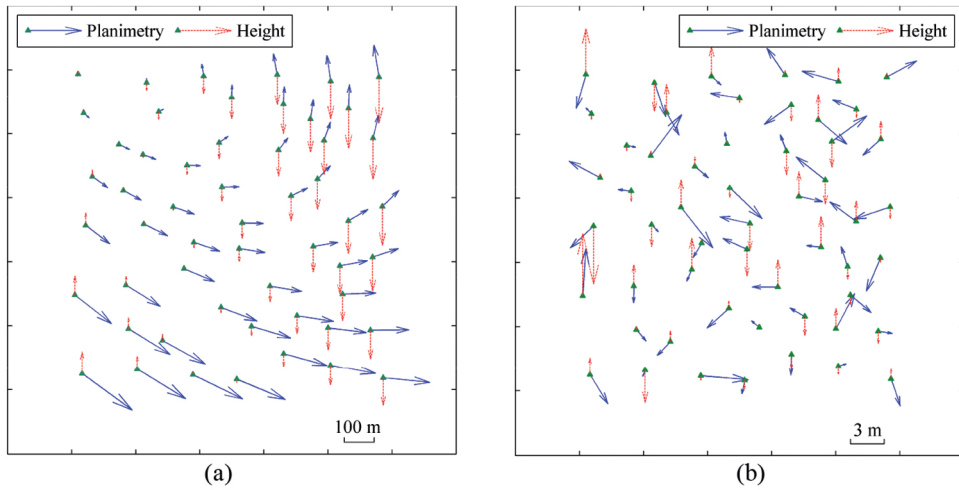


Fig. 5: Residual error distributions of the ICPs after the tri-stereo model orientation with: (a) layout L4, (b) layout L8 in the dataset 1.

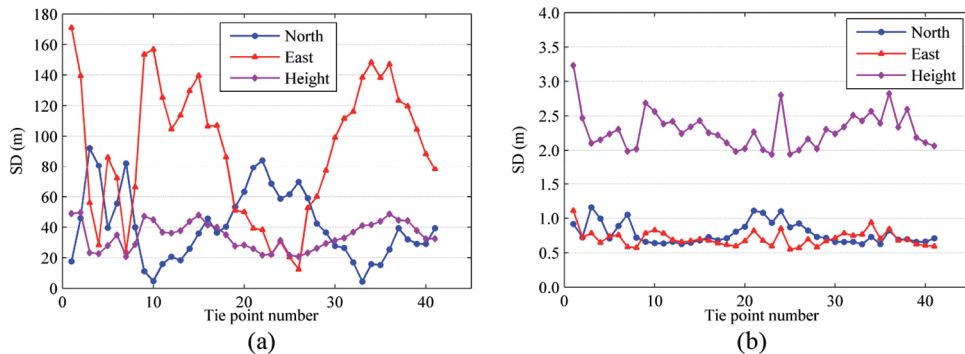


Fig. 6: SDs of the tie points after the tri-stereo model orientation with: (a) layout L4, (b) layout L8 in the dataset 1.

From the above experiments, it can be concluded that performing the tri-stereo model orientation using GCLs is feasible and effective. With eight GCLs near the image boundary, the orientation can achieve an accuracy of better than 1 GSD, which is almost the same as the one achieved using GCPs. Therefore, in the areas where it is difficult to identify highly accurate GCPs, using GCLs to perform the image orientation can offer an alternative solution for the precise HRSI orientation. Especially, if the control information is extracted from the existing topographical maps, GCLs will be preferable to GCPs. The existing topographical maps have much more linear features than point features and a complete match

between the line in the satellite image and the one in the topographical maps is unnecessary, so it will be feasible to extract GCLs and not to extract GCPs.

3.3 Effects of the Directions of GCLs on the Tri-Stereo Model Orientation Using GCLs

Different from GCPs, the directions of GCLs is another important factor that might affect the tri-stereo model orientation. In order to analyse the effects of the directions of GCLs, the angle θ of GCLs in image space is divided into four ranges: $[-90^\circ, -45^\circ)$, $[-45^\circ, 0^\circ)$, $[0^\circ, 45^\circ]$ and

[45°, 90°]. The layout L8 in section 3.2 continued to be used, but ten groups of eight GCLs with different angles, as listed in Tab. 5, were tested. The RMSE of the ICPs was listed in Tabs. 6 and 7. It is noted that in Tabs. 6 and 7, the angles of the used GCLs in only the NAD images were listed and the angles in the FWD and BWD images are almost the same as those in the NAD images.

In Tabs. 6 and 7, with the groups G1, G2, G3 and G4, for both datasets the best orientation accuracy achieved is about 1 GSD and the worst accuracy is about 3 GSD. In fact, when the angles of eight GCLs all lie in only one angle range [-90°, -45°], [-45°, 0°], [0°, 45°] or [45°, 90°], that is, when the difference between the angles is small, the offset and scaling of the affine transformation model (ATM) may be poorly defined, and as a result, the orientation accuracy is unstable. When the angles of eight GCLs are distributed evenly in two or three angle ranges, the offset and scaling

of the ATM can be restrained and the orientation accuracy can be improved to a satisfactory level. For both datasets, the orientation accuracies achieved with the groups G12, G13, G14, G123, G124 and G134 are all better than 1 GSD. Hence, in order to achieve a satisfactory orientation accuracy, it is recommended that the angles of eight GCLs in the layout L8 should be distributed evenly in at least two out of the four angle ranges.

3.4 Effects of the Lengths of GCLs on the Tri-Stereo Model Orientation Using GCLs

Similarly, in order to analyse the effects of the lengths of GCLs on the tri-stereo model orientation, eight GCLs in the layout L8 in section 3.2 are used, but the lengths of the eight GCLs were changed into [40, 60], [80, 100], [120, 140], [160, 180] and [200, 220] m, respectively.

Tab. 5: Ten groups of eight GCLs with different angles.

Group	Number of GCLs in [-90°, -45°]	Number of GCLs in [-45°, 0°]	Number of GCLs in [0°, 45°]	Number of GCLs in [45°, 90°]
G1	8	0	0	0
G2	0	8	0	0
G3	0	0	8	0
G4	0	0	0	8
G12	4	4	0	0
G13	4	0	4	0
G14	4	0	0	4
G123	2	3	3	0
G124	2	3	0	3
G134	2	0	3	3

Tab. 6: Tri-stereo model orientation results using the GCLs in the dataset 1.

Group	Angles of GCLs in the NAD image (°)	Number of ICPs	RMSE (m)			
			North	East	Planimetry	Height
G1	-86, -80, -78, -74, -69, -66, -65, -61	54	2.258	2.507	3.374	3.391
G2	-35, -33, -25, -20, -17, -11, -11, -5	54	6.159	4.014	7.351	2.137
G3	13, 18, 23, 23, 24, 30, 33, 40	54	5.261	1.782	5.555	1.954
G4	57, 67, 70, 73, 78, 79, 84, 86	54	4.216	8.802	9.760	11.195
G12	-78, -66, -65, -61; -35, -25, -17, -5	54	2.205	2.055	3.014	2.238
G13	-78, -66, -65, -61; 13, 23, 33, 40	54	2.333	1.864	2.986	2.283
G14	-78, -66, -65, -61; 67, 73, 84, 86	54	2.375	2.256	3.276	2.125
G123	-78, -65; -35, -17, -5; 24, 30, 33	54	2.062	1.926	2.822	2.246
G124	-78, -65; -35, -17, -5; 67, 78, 79	54	2.054	2.168	2.986	2.381
G134	-78, -65; 13, 23, 40; 67, 78, 79	54	2.206	2.210	3.122	2.302

Tab. 7: Tri-stereo model orientation results using the GCLs in the dataset 2.

Group	Angles of GCLs in the NAD image (°)	Number of ICPs	RMSE (m)			
			North	East	Planimetry	Height
G1	-86, -85, -82, -78, -60, -57, -57, -56	47	2.504	5.978	6.481	9.212
G2	-42, -27, -26, -22, -12, -10, -10, -6	47	4.569	2.616	5.265	1.971
G3	4, 5, 6, 18, 19, 33, 35, 44	47	3.038	1.508	3.392	2.384
G4	63, 65, 69, 76, 78, 78, 78, 81	47	3.673	5.682	6.766	6.393
G12	-85, -82, -57, -56; -42, -27, -26, -10	47	1.664	2.600	3.087	2.442
G13	-85, -82, -57, -56; 4, 6, 33, 44	47	1.635	2.529	3.011	2.177
G14	-85, -82, -57, -56; 65, 69, 76, 78	47	2.157	1.902	2.876	2.434
G123	-85, -56; -10, -27, -42; 18, 27, 33	47	1.342	2.432	2.778	2.034
G124	-85, -56; -10, -27, -42; 65, 78, 81	47	2.108	1.968	2.884	2.251
G134	-85, -56; 4, 6, 44; 65, 78, 81	47	2.162	1.855	2.848	2.414

After the tri-stereo model orientation, the RMSE of the ICPs was listed in Tabs. 8 and 9. In Tabs. 8 and 9, the orientation accuracy changes slightly when the lengths of the GCLs increase. For both datasets, the difference between the accuracy achieved with the GCLs in [40, 60] m and that achieved with the GCLs in [200, 220] m is smaller than 0.1 m in both pla-

nimetry and height. It can be concluded that the lengths of GCLs have almost no effect on the tri-stereo model orientation when eight GCLs with a good distribution of directions are used, so the orientation using GCLs can be performed conveniently for users. In real imagery, however, it may be difficult to find very long features, e.g. road or river edges,

Tab. 8: Tri-stereo model orientation results using the GCLs in the dataset 1.

Layout	Lengths of GCLs in object space (m)	Number of ICPs	RMSE (m)			
			North	East	Planimetry	Height
L8	[40, 60]	54	1.987	1.974	2.801	2.088
L8	[80, 100]	54	1.868	2.059	2.780	2.156
L8	[120, 140]	54	1.974	1.981	2.797	2.087
L8	[160, 180]	54	2.027	2.029	2.868	2.164
L8	[200, 220]	54	2.131	1.956	2.893	2.023

Tab. 9: Tri-stereo model orientation results using the GCLs in the dataset 2.

Layout	Lengths of GCLs in object space (m)	Number of ICPs	RMSE (m)			
			North	East	Planimetry	Height
L8	[40, 60]	47	1.553	2.188	2.683	2.155
L8	[80, 100]	47	1.729	2.099	2.719	2.107
L8	[120, 140]	47	1.821	2.122	2.796	2.167
L8	[160, 180]	47	1.939	1.993	2.780	2.123
L8	[200, 220]	47	1.773	2.134	2.775	2.154

that are strictly linear and, thus, can be used as GCLs. Our results show that using relatively short GCPs of a length of about 15–20 pixels are sufficient to obtain a good orientation accuracy.

3.5 Accuracy Analysis of the Tri-Stereo Model Orientation Combining GCPs and GCLs

The experiments described in the previous sections have already shown that four GCPs in the image corners or eight GCLs near the image boundary whose angles are distributed evenly in at least two out of the four angle ranges are sufficient for tri-stereo model orientation. However, it may be difficult to employ only GCPs or GCLs for the orientation in some cases. In comparison, performing the tri-stereo model orientation combining GCPs and GCLs may be a much better solution. Theoretically, no less than three GCPs, two GCPs and one GCLs, or one GCP and two GCLs are required in the tri-stereo model orientation of ZY-3 images, but more observations are required for a stable solution. Based on these considerations, seven layout scenarios were designed to evaluate the feasibility of the orientation combining GCPs and GCLs:

- (1) *Layout P3L1*. Three GCPs in three image corners and one GCL in the fourth image corner, as shown in Fig. 7a;
- (2) *Layout P3L15*. Three GCPs in three image corners and fifteen GCLs distributed evenly in the image;
- (3) *Layout P2L2*. Two GCPs in two image corners and two GCLs in the other two image corners, as shown in Fig. 7b;
- (4) *Layout P2L15*. Two GCPs in two image cor-

ners and fifteen GCLs distributed evenly in the image;

- (5) *Layout P1L3*. One GCP in one image corner and three GCLs in the other three image corners, as shown in Fig. 7c;
- (6) *Layout P1L5*. One GCP in one image corner, three GCLs in the other three image corners and two GCLs near the image boundary, as shown in Fig. 7d; and
- (7) *Layout P1L15*. One GCP in one image corner and fifteen GCLs distributed evenly in the image.

Combining GCPs and GCLs, one can theoretically determine the offset of the ATM effectively, but cannot always restrain the scaling of the ATM. For example, the scaling may happen in the column direction in Fig. 8a and in the row direction in Fig. 8b, so the normal equation matrix of the least-squares adjustment will be ill-conditioned. Even if the normal equations can be solved because the lines are not exactly parallel, the ATPs thus determined and the object coordinates of tie points will be very uncertain. In order to obtain a stable orientation accuracy, the directions of GCLs should differ enough to restrain the scaling of the ATM.

Based on the analysis of the previous paragraph, for both datasets in Fig. 3, the GCPs and GCLs were selected according to the above layout scenarios and the remaining GCPs were also considered as the ICPs. In each layout, the selected GCLs have different angles, as listed in Tabs. 10 and 11, so that the effects of the directions of GCLs can also be demonstrated conveniently. After the tri-stereo model orientation according to the procedure in section 2.3, the RMSE of the ICPs was calculated and listed in Tabs. 10 and 11.

From the results in Tabs. 10 and 11, the fol-

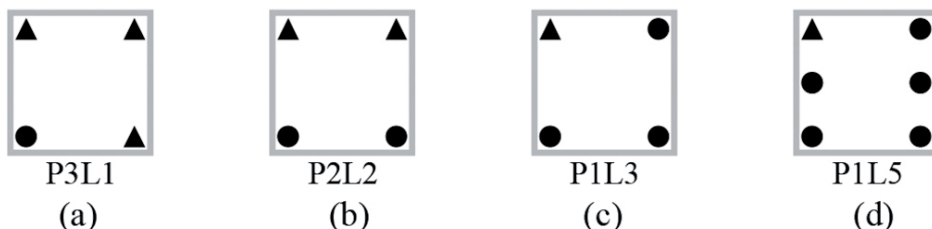


Fig. 7: GCP and GCL layout scenarios: (a) three GCPs and one GCL, (b) two GCPs and two GCLs, (c) one GCP and three GCLs, (d) one GCP and five GCLs. Note that ▲ denotes GCPs and ● denotes GCLs.

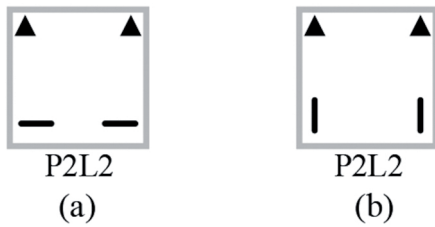


Fig. 8: GCP and GCL layout scenarios: (a) two GCPs and two GCLs, (b) two GCPs and two GCLs. Note that \blacktriangle denotes GCPs and $—$ denotes GCLs.

lowing three conclusions can be drawn. First, combining three GCPs and one GCL in the layout P3L1, or two GCPs and two GCLs in the layout P2L2 can achieve an orientation accuracy of better than 1 GSD, which is almost the same as the one achieved using four GCPs. Moreover, the accuracy is also not improved noticeably when the number of GCLs is increased. Of course, it should be pointed out that for the layout P3L1, the angle of one GCL can be in any of the four angle ranges, but in this case the GCL only gives redundant information, because the ATPs can already be determined from the GCPs. For the layout P2L2, however, the angles of two GCLs should lie in two different angle ranges. When the difference between the angles of the GCLs is too small,

the offset and scaling of the ATM may be determined poorly. Consequently, the ATPs and the object space coordinates of the tie points will be very uncertain, indicated by large SDs. Overall, it is feasible and effective to substitute GCLs for the absent GCPs when performing tri-stereo model orientation if GCPs can only be identified in one or two out of the four image corners.

Second, a satisfactory orientation accuracy cannot be achieved combining one GCP and three GCLs in the layout PIL3, even if the angles of three GCLs are distributed evenly in three angle ranges. Taking dataset 1 as an example, the orientation accuracy achieved with the layout PIL3 is as large as 81.2 m in planimetry and 81.5 m in height. The reason is that the control information provided by one GCP and three GCLs is insufficient for a stable tri-stereo model orientation. Accordingly, the offset of the ATM can be restrained effectively by the GCP, but the scaling of the ATM still exists, which can be shown by Tab. 12 and Fig. 9a. The SDs of the shift parameters e_0 and f_0 are better than 1.0 pixel. The SDs of the other ATPs reach only about $1.0E-3$, which is much worse than that achieved with the layout P4. Meanwhile, the largest SD of the tie points reaches about 100 m.

Tab. 10: Tri-stereo model orientation results combining the GCPs and GCLs in the dataset 1.

Layout	Angles of GCLs in the NAD image (°)	Number of ICPs	RMSE (m)			
			North	East	Planimetry	Height
P3L1	-78	51	1.808	1.933	2.647	2.132
P3L1	-33	51	1.811	1.943	2.657	2.171
P3L15	-86, -84, -78, -66, -65, -59; -20, -11, -5; 30, 40; 55, 73, 74	51	2.286	1.757	2.883	1.991
P2L2	23, 40	52	5.171	2.038	5.558	6.663
P2L2	-78; 40	52	1.916	1.920	2.712	2.236
P2L2	-78; -35	52	1.849	2.017	2.736	2.116
P2L15	-86, -84, -78, -66, -65, -59; -20, -11, -5; 30, 40; 55, 73, 74	52	2.251	1.735	2.842	2.016
P1L3	-78; -35; 33	53	56.672	58.123	81.179	81.515
P1L5	-86, -78, -74, -65, -61	53	2.349	3.277	4.032	2.724
P1L5*	-86, -78, -65; -35, -11	53	2.061	2.450	3.202	2.247
P1L5	-86, -78, -65; 30, 40	53	2.035	1.755	2.687	2.366
P1L15	-86, -84, -78, -66, -65, -59; -20, -11, -5; 30, 40; 55, 73, 74	53	2.300	1.753	2.892	2.002

Tab. 11: Tri-stereo model orientation results combining the GCPs and GCLs in the dataset 2.

Layout	Angles of GCLs in the NAD image (°)	Number of ICPs	RMSE (m)			
			North	East	Planimetry	Height
P3L1	81	44	1.787	2.094	2.753	2.131
P3L1	18	44	1.803	1.773	2.528	2.025
P3L15	-89, -57; -42, -35, -27, -12, -10, -6; 19, 33; 61, 65, 77, 78, 81	44	1.309	1.576	2.049	2.021
P2L2	69; 81	45	3.187	4.014	5.125	13.506
P2L2	16; 81	45	2.701	1.528	3.103	2.089
P2L2	-6; 81	45	2.022	2.124	2.933	2.668
P2L15	-89, -57; -42, -35, -27, -12, -10, -6; 19, 33; 61, 65, 77, 78, 81	45	1.518	1.668	2.256	2.010
P1L3	-26; 16; 81	46	14.641	7.166	16.300	10.714
P1L5	65, 69, 76, 78, 81	46	2.218	2.925	3.670	6.084
P1L5	-6, -10, -12; 65, 81	46	1.437	2.378	2.778	2.316
P1L5	5, 16, 30; 65, 81	46	2.256	1.734	2.846	2.128
P1L15	-89, -57; -42, -35, -27, -12, -10, -6; 19, 33; 61, 65, 77, 78, 81	46	1.494	1.819	2.354	1.992

Tab. 12: The solved ATPs of the NAD image in the dataset 1.

Layout	e_0 (pixels) (SD)	e_1 (SD)	e_2 (SD)	f_0 (pixels) (SD)	f_1 (SD)	f_2 (SD)
P4	9.519E+0 (2.463E-1)	-9.224E-5 (1.177E-5)	7.626E-6 (1.125E-5)	-8.825E+0 (2.389E-1)	4.280E-5 (1.144E-5)	-1.258E-5 (1.094E-5)
P1L3	8.005E+0 (7.871E-1)	-2.023E-3 (1.068E-3)	-1.384E-3 (7.527E-4)	-8.041E+0 (2.892E-1)	3.002E-3 (1.549E-3)	-2.376E-3 (1.215E-3)
P1L5*	8.900E+0 (2.521E-1)	-7.715E-5 (2.005E-5)	7.797E-5 (2.842E-5)	-8.207E+0 (2.648E-1)	-4.268E-5 (1.306E-5)	1.835E-5 (1.477E-5)
P1L15	9.184E+0 (1.805E-1)	-3.938E-6 (9.232E-6)	-7.969E-5 (9.307E-6)	-7.686E+0 (1.208E-1)	-3.021E-6 (7.386E-6)	-1.960E-5 (6.694E-6)

Note: The layout P1L5* corresponds with the layout P1L5* in Tab. 10.

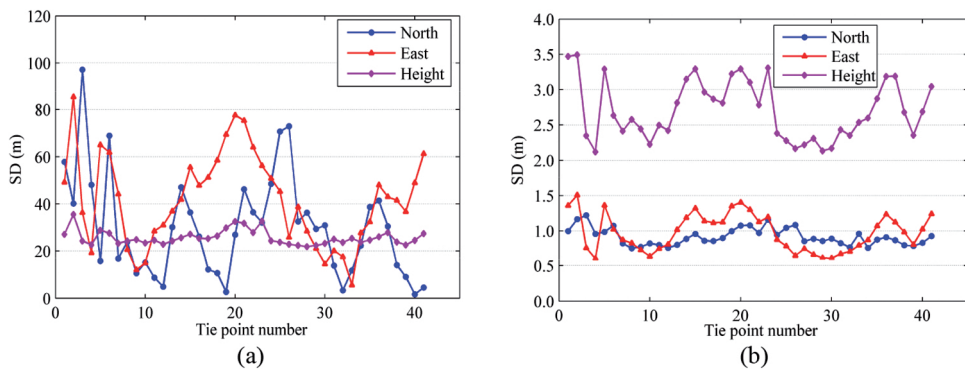


Fig. 9: SDs of the tie points after the tri-stereo model orientation with: (a) layout P1L3, (b) layout P1L5 in the dataset 1.

The offset and scaling of the ATM can be determined effectively in a tri-stereo model orientation combining one GCP and five GCLs, as shown in Tab. 12. The orientation can achieve a satisfactory accuracy of better than 1 GSD, which is consistent with the SDs of the tie points, as shown in Fig. 9b. The angles of five GCLs should also be distributed evenly in at least two out of the four angle ranges. Moreover, the accuracy is not improved noticeably any more as the number of GCLs increases from five to fifteen. Therefore, if only one GCP is available in the image corners, no less than five GCLs near the image boundary are necessary in order to obtain a satisfactory orientation accuracy.

From the above results, it can be concluded that in the image-covered areas where sufficient GCPs in the image corners are unavailable, GCLs can be considered as a substitute for the absent GCPs and a satisfactory orientation accuracy of better than 1 GSD, almost the same as the one achieved using GCPs, can be achieved.

4 Conclusions

In this paper, using the geometric constraint that an observed line and a projected line in image space are bound to coincide, a line-based orientation model of HRSI is established. On the basis of the point-based and line-based models, a feasible and effective tri-stereo model orientation approach combining GCPs and GCLs is presented. Compared to the line-based orientation models established based on the PSM, the model proposed in this paper is based on the RFM. This means that only the RPCs rather than the satellite's position and attitude observations and sensor parameters are needed for the presented approach. Hence, the presented approach is more convenient and practicable for HRSI users to perform the tri-stereo model orientation combining GCPs and GCLs.

Compared with point features, the control information from linear features can be used even without a complete match between image and object features. That is to say, only the image line needs to correspond with the object line whilst the correspondence between the

points on the two lines is not necessary. The experimental results achieved for two ZY-3 datasets have shown that if it is difficult to identify four GCPs in the image corners, GCLs can be employed to substitute for the absent GCPs in the tri-stereo model orientation; more specially, a satisfactory orientation accuracy can be achieved combining three GCPs and one GCL, two GCPs and two GCLs, or one GCP and five GCLs. Additionally, if the control information is obtained from existing topographical maps, it will be feasible to extract GCLs and not to extract GCPs due to the abundant linear features in the topographical maps. In this case, it is possible just to use GCLs as control information for the tri-stereo model orientation, and a satisfactory accuracy can be achieved using eight GCLs evenly distributed near the image boundaries. With respect to the directions of GCLs, in order to restrain the offset and scaling of the ATM effectively and to determine the ATPs and the object coordinates of the tie points precisely, the angles of GCLs should be distributed evenly in at least two out of the four angle ranges, independently of whether the tri-stereo model orientation is performed using only GCLs or combining GCPs and GCLs.

Due to the restriction of HRSI datasets, only two ZY-3 datasets were tested in this paper. The feasibility and effectiveness of the presented orientation approach combining GCPs and GCLs still needs to be validated further using very high resolution satellite images from the newest generation. Besides, the image and object coordinates of the GCPs and GCLs are all measured manually in this paper, which is very time-consuming. Hence, the automation of the presented approach, which can be based on automated point and/or line extraction in both, an existing DOM and the HRSI, followed by a matching stage, needs to be studied further.

Acknowledgement

This work was supported by the national basic research program of China (973 program) (Grant No. 2012CB719902).

References

- FRASER, C.S., HANLEY, H.B. & YAMAKAWA, T., 2002: Three-dimensional geopositioning accuracy of IKONOS imagery. – *Photogrammetric Record* **17** (99): 465–479.
- FRASER, C.S. & HANLEY, H.B., 2005: Bias-compensated RPCs for sensor orientation of high-resolution satellite imagery. – *Photogrammetric Engineering & Remote Sensing* **71** (8): 909–915.
- FRASER, C.S., DIAL, G. & GRODECKI, J., 2006: Sensor orientation via RPCs. – *ISPRS Journal of Photogrammetry and Remote Sensing* **60** (3): 182–194.
- GRODECKI, J. & DIAL, G., 2003: Block adjustment of high-resolution satellite images described by rational polynomials. – *Photogrammetric Engineering & Remote Sensing* **69** (1): 59–68.
- HABIB, A.F., LIN, H.T. & MORGAN, M.F., 2003: Autonomous space resection using point- and line-based representation of free-form control linear features. – *Photogrammetric Record* **18** (103): 244–258.
- HABIB, A.F. & ALRUZOUQ, R.I., 2004: Line-based modified iterated hough transform for automatic registration of multi-source imagery. – *Photogrammetric Record* **19** (105): 5–21.
- HABIB, A.F., MORGAN, M.F., KIM, E.M. & CHENG, R., 2004: Linear features in photogrammetric activities. – *International Archives of Photogrammetry, Remote Sensing and Spatial Information Sciences* **35** (B2): 610–615.
- KARJALAINEN, M., HYYPPÄ, J. & KUITTINEN, R., 2006: Determination of exterior orientation using linear features from vector maps. – *Photogrammetric Record* **21** (116): 329–341.
- MARCATO JUNIOR, J. & TOMMASELLI, A.M.G., 2013: Exterior orientation of CBERS-2B imagery using multi-feature control and orbital data. – *ISPRS Journal of Photogrammetry and Remote Sensing* **79**: 219–225.
- MASRY, S.E., 1981: Digital mapping using entities: a new concept. – *Photogrammetric Engineering & Remote Sensing* **47** (11): 1561–1565.
- NAGASUBRAMANIAN, V., RADHADEVI, P.V., RAMACHANDRAN, R. & KRISHNAN, R., 2007: Rational function model for sensor orientation of IRS-P6 LISS-4 imagery. – *Photogrammetric Record* **22** (120): 309–320.
- SCHENK, T., 2004: From point-based to feature-based aerial triangulation. – *ISPRS Journal of Photogrammetry and Remote Sensing* **58** (5): 315–329.
- SHI, W. & SHAKER, A., 2006: The line-based transformation model (LBTM) for image-to-image registration of high-resolution satellite image data. – *International Journal of Remote Sensing* **27** (14): 3001–3012.
- TAO, C.V. & HU, Y., 2001: A comprehensive study of the rational function model for photogrammetric processing. – *Photogrammetric Engineering & Remote Sensing* **67** (12): 1347–1357.
- TAO, C.V., HU, Y. & JIANG, W., 2004: Photogrammetric exploitation of IKONOS imagery for mapping applications. – *International Journal of Remote Sensing* **25** (14): 2833–2853.
- TOMMASELLI, A.M.G. & MEDEIROS, N.G., 2010: Determination of the indirect orientation of orbital pushbroom images using control straight lines. – *Photogrammetric Record* **25** (130): 159–179.
- TOMMASELLI, A.M.G. & MARCATO JUNIOR, J., 2012: Bundle block adjustment of CBERS-2B HRC imagery combining control points and lines. – *PGF – Photogrammetrie, Fernerkundung, Geoinformation* **2**: 129–139.
- YUAN, X. & LIN, X., 2008: A method for solving rational polynomial coefficients based on ridge estimation. – *Geomatics and Information Science of Wuhan University* **33** (11): 1130–1133.
- YUAN, X. & LIU, X., 2009: A novel matching method for high resolution satellite imagery based on rational function model. – *Geomatics and Information Science of Wuhan University* **34** (6): 671–674.
- ZHANG, J., ZHANG, H. & ZHANG, Z., 2004: Exterior orientation for remote sensing image with high resolution by linear feature. – *International Archives of Photogrammetry and Remote Sensing* **35** (B3): 76–79.
- ZHANG, L., ZHANG, J., CHEN, X. & AN, H., 2009: Block-adjustment with SPOT-5 imagery and sparse GCPs based on RFM. – *Acta Geodaetica et Cartographica Sinica* **38** (4): 302–310.
- ZHANG, Y., HU, B. & ZHANG, J., 2011: Relative orientation based on multiple conjugate features. – *ISPRS Journal of Photogrammetry and Remote Sensing* **66** (5): 700–707.

Address of the authors:

Dr. JINSHAN CAO, Collaborative Innovation Center of Geospatial Technology, 129 Luoyu Road, Wuhan, China, CN-430079, Tel: +86-27-68771228, Fax: +86-27-68771228, e-mail: caojs@whu.edu.cn

Prof. Dr. XIUXIAO YUAN, School of Remote Sensing and Information Engineering, Wuhan University, 129 Luoyu Road, Wuhan, China, CN-430079, Tel: +86-27-68771228, Fax: +86-27-68771228, e-mail: yuanxx@whu.edu.cn

Dr. YI FANG, School of Remote Sensing and Information Engineering, Wuhan University, 129 Luoyu Road, Wuhan, China, CN-430079, Tel: +86-27-68771228, Fax: +86-27-68771228, e-mail: fywhu@qq.com

Manuskript eingereicht: Dezember 2015
Angenommen: April 2016